The Astrophysical Journal, 682:400–407, 2008 July 20

INVERSE COMPTON ORIGIN OF THE HARD X-RAY AND SOFT GAMMA-RAY EMISSION FROM THE GALACTIC RIDGE

Troy A. Porter
Santa Cruz Institute for Particle Physics, University of California, Santa Cruz, CA 95064

Igor V. Moskalenko[1]
Hansen Experimental Physics Laboratory, Stanford University, Stanford, CA 94305

Andrew W. Strong and Elena Orlando
Max-Planck-Institut für extraterrestrische Physik, Postfach 1312, D-85741 Garching, Germany

and

L. Bouchet
CESR-CNRS, 9 Avenue du Colonel Roche, 31028 Toulouse Cedex 04, France
Received 2007 November 30; accepted 2008 April 10

ABSTRACT

A recent redetermination of the nonthermal component of the hard X-ray to soft γ-ray emission from the Galactic ridge, using the SPI instrument on the *International Gamma-Ray Astrophysics Laboratory* (*INTEGRAL*), is shown to be well reproduced as inverse Compton emission from the interstellar medium. Both cosmic-ray primary electrons and secondary electrons and positrons contribute to the emission. The prediction uses the GALPROP model and includes a new calculation of the interstellar radiation field. This may solve a long-standing mystery of the origin of this emission, and potentially opens a new window on Galactic cosmic rays.

Subject headings: cosmic rays — elementary particles — gamma rays: theory

Online material: color figures

1. INTRODUCTION

The Galactic ridge is known to be an intense source of continuum hard X- and γ-ray emission. The hard X-ray emission was discovered in 1972 (Bleach et al. 1972), and interstellar emission has subsequently been observed by *HEAO-1*, *Tenma* (*ASTRO-B*), *ASCA*, *Ginga*, *RXTE*, OSSE (Worrall et al. 1982; Koyama et al. 1986; Purcell et al. 1996; Kinzer et al. 1999, 2001), and most recently by *Chandra* and *XMM-Newton*. The γ-ray observations started with the *OSO-III* satellite in 1968, followed by *SAS-2* in 1972, *COS-B* (1975–1982), and COMPTEL and EGRET on the *CGRO* (1991–2000). With COMPTEL and EGRET the improvement in data quality was sufficient to allow such studies to be performed in much greater detail. The Galactic diffuse emission is a major study objective for *INTEGRAL* (in orbit since 2002) and the *GLAST* LAT (to be launched in 2008) (Michelson 2007; Ritz 2007). Each of these experiments represents a significant leap forward with respect to its predecessor.

Continuum emission of diffuse, interstellar nature is expected in the hard X-ray and γ-ray regime from the physical processes of positron annihilation (through intermediate formation of positronium), inverse Compton (IC) scattering and bremsstrahlung from cosmic-ray (CR) electrons and positrons, and via decay of neutral pions produced by interactions of CR nuclei with the interstellar gas. Positron annihilation in flight (continuum) may contribute in the few MeV range (Beacom & Yüksel 2006). For the non–positronium continuum, hard X-rays from bremsstrahlung emission imply a luminosity in CR electrons which is unacceptably large (see e.g., Dogiel et al. 2002). Composite models have been proposed which incorporate thermal and nonthermal components from electrons accelerated in supernovae or the ambient interstellar turbulence (Valinia et al. 2000). At MeV energies the origin of the emission is also uncertain (Strong et al. 2000).

Alternatively, the origin of the ridge emission could be attributed to a population of sources too weak to be detected individually, and hence would not be truly interstellar. In general, γ-ray telescopes have inadequate spatial resolution to clarify this issue. For X-rays, important progress in this area was made by *ASCA* (Kaneda et al. 1997) and *Ginga* (Yamasaki et al. 1997). More recently, high-resolution imaging in X-rays (2–10 keV) with *Chandra* (Ebisawa et al. 2001, 2005) has claimed to prove the existence of a truly diffuse component. Similarly, it has been claimed from an analysis of *XMM-Newton* data (Hands et al. 2004) that 80% of the Galactic-ridge X-ray emission is probably diffuse, and only 9% can be accounted for by Galactic sources, the rest being extragalactic in nature. However, more recently Revnivtsev et al. (2006) with *RXTE* PCA data, and Krivonos et al. (2007) using *INTEGRAL* IBIS and *RXTE* data, argue convincingly that below 50 keV all the "diffuse" emission can be accounted for by a Galactic population of sources, mainly magnetic cataclysmic variables; see also Revnivtsev & Sazonov (2007) and Revnivtsev et al. (2007).

At higher energies, an extensive study of the diffuse Galactic γ-ray emission in the context of CR propagation models has been carried out by Strong et al. (2000, 2004b). This study confirmed that models based on locally measured electron and nuclei spectra and synchrotron constraints are consistent with γ-ray measurements in the 30 MeV–500 MeV range; outside this range deviations from the data are apparent. The puzzling excess in the EGRET diffuse emission data above 1 GeV relative to that expected (Strong et al. 2000; Hunter et al. 1997) has shown up in all models that are tuned to be consistent with the locally measured CR nuclei and electron spectra (Moskalenko et al. 2004; Strong et al. 2004b).

[1] Also Kavli Institute for Particle Astrophysics and Cosmology, Stanford University, Stanford, CA 94309.

The excess has shown up in all directions, not only in the Galactic plane. This implies that the GeV excess is not a feature restricted to the Galactic ridge or the gas-related emission. A simple rescaling of the components (π^0-decay, IC, bremsstrahlung) does not improve the fit in any region, since the observed peak is at an energy higher than the π^0-peak. For recent reviews, see Moskalenko et al. (2004) and Strong et al. (2007) and references therein.

Assuming that the GeV excess is not an instrumental artifact, [2] the so-called "optimized model," which explains the GeV excess in terms of CR intensity variations in the Galaxy, has been proposed by Strong et al. (2004b). It reproduces the spectrum of the diffuse γ-rays in *all directions*, as well as the latitude and longitude profiles for the whole EGRET energy range 30 MeV–50 GeV at the cost of relaxation of the restrictions imposed by the measurements of local CR proton and electron spectra. At lower energies, the predictions of this model have never been tested because of the lack of good data.

The study of the Galactic-ridge continuum X-ray emission is a key goal of the *INTEGRAL* mission. The high spectral resolution combined with its imaging capabilities promises new insights into the nature of this enigmatic radiation. Previous work based on initial, smaller sets of *INTEGRAL* SPI observations have reported the detection of diffuse emission at a level consistent with previous experiments (Strong et al. 2003; Strong 2003). However, statistical and systematic errors were large, due in part to the uncertainty in the point-source contribution. Meanwhile, a new analysis of *INTEGRAL* IBIS data (Lebrun 2004; Terrier et al. 2004) showed that, up to 100 keV, indeed a large fraction of the total emission from the inner Galaxy is due to sources. Strong et al. (2004c) used the source catalog from this work (containing 91 sources) as input to SPI model fitting, giving a more solid basis for the contribution of point sources in such an analysis. This exploited the complementarity of the instruments on *INTEGRAL* for the first time in the context of diffuse emission. The SPI analysis by Bouchet et al. (2005) gave a rather lower 50–1000 keV power-law continuum than Strong et al. (2005), but the errors were large in the early data sets. Now, a new analysis (Bouchet et al. 2008) with 3 times as much SPI exposure gives better statistics, background handling, and point-source subtraction.

In the present paper we focus on energies above 50 keV where sources do not appear to be important because of the rapid cutoff in the spectra of the majority, and the relatively small number of hard-spectrum sources. We use the GALPROP model together with a new model for the Galactic interstellar radiation field (ISRF) to solve a long-standing mystery of the origin of the hard X-ray emission—IC emission from CR electrons and positrons—and to build a model of the Galactic diffuse emission in the energy range from keV to TeV energies, thus covering more that 10 orders of magnitude in energy.

Primary CR electrons are directly accelerated in CR sources like supernova remnants or pulsars. Secondary electrons and positrons are produced via interactions of energetic nuclei with interstellar gas, and are usually considered a minor component of CRs. This is indeed the case in the heliosphere, where the positron to all-electron ratio is small at all energies, $e^+/(e^+ + e^-)_{\rm tot} \sim 0.1$. However, as we show, the combined secondary electron/positron flux in the interstellar medium (ISM) is more than half of the primary CR electron flux at $\sim$1 GeV energies and below. This leads to a considerable contribution by secondary positrons and electrons to the diffuse γ-ray flux via IC scattering and bremsstrahlung and significantly, by up to a factor of $\sim$2, increases the flux of diffuse Galactic emission below $\sim$100 MeV. Secondary positrons and electrons are, therefore, directly seen in hard X-rays and γ-rays.

2. GALPROP CODE

The GALPROP code (Strong & Moskalenko 1998) was created to enable simultaneous predictions of all relevant observations including CR nuclei, electrons and positrons, γ-rays, and synchrotron radiation.

We give a very brief summary of GALPROP; for details we refer the reader to the relevant papers (Strong et al. 2000, 2004b; Moskalenko & Strong 1998, 2000; Moskalenko et al. 2002; Strong & Moskalenko 1998; Ptuskin et al. 2006) and the dedicated World Wide Web site.[3] The GALPROP code solves the CR transport equation with a given source distribution and boundary conditions for all CR species. This includes a galactic wind (convection), diffusive reacceleration in the ISM, energy losses, nuclear fragmentation, radioactive decay, and production of secondary particles and isotopes. The numerical solution of the transport equation is based on a Crank-Nicholson (Press et al. 1992) implicit second-order scheme. The spatial boundary conditions assume free particle escape. Since the grid involves a three-dimensional (R, z, p) or four-dimensional (x, y, z, p) problem (spatial variables plus momentum) "operator splitting" is used to handle the implicit solution. For a given halo size the diffusion coefficient, as a function of momentum and the reacceleration or convection parameters, is determined by the boron-to-carbon ratio data. If reacceleration is included, the momentum-space diffusion coefficient D_{pp} is related to the spatial coefficient D_{xx} $(= \beta D_0 \rho^\delta)$ (Berezinskii et al. 1990; Seo & Ptuskin 1994), where $\delta = \frac{1}{3}$ for a Kolmogorov spectrum of interstellar turbulence or $\delta = \frac{1}{2}$ for a Kraichnan cascade, ρ is the magnetic rigidity, D_0 is a constant, and $\beta = v/c$. Production of secondary positrons and electrons is calculated using a formalism described in Moskalenko & Strong (1998) with a correction by Kelner et al. (2006). The γ-rays are calculated using the propagated CR distributions, including a contribution from secondary particles such as positrons and electrons from inelastic processes in the ISM that increases the γ-ray flux at MeV energies (Strong et al. 2004b). Gas-related γ-ray intensities are computed from the emissivities as a function of (R, z, E_γ) using the column densities of H I and H_2 for galactocentric annuli based on 21 cm and CO surveys included in the GALPROP model. Neutral pion production is calculated using the method given by Dermer (1986a, 1986b) as described in Moskalenko & Strong (1998) or using a parameterization developed by Kamae et al. (2005); bremsstrahlung is calculated using a formalism by Koch & Motz (1959) as described in Strong et al. (2000). The IC scattering is treated using the appropriate cross section for an anisotropic radiation field developed by Moskalenko & Strong (2000) using the full angular distribution of the ISRF.

Cross-sections are based on the extensive LANL database, nuclear codes, and parameterizations (Mashnik et al. 2004). Starting with the heaviest primary nucleus considered (e.g., ^{64}Ni) the propagation solution is used to compute the source term for its spallation products, which are then propagated in turn, and so on down to protons, secondary electrons and positrons, and antiprotons. The inelastically scattered protons and antiprotons are treated as separate components (secondary protons, tertiary

[2] A discussion of uncertainties and possible sources of error associated with determining the diffuse Galactic γ-ray emission using EGRET data is available in Moskalenko et al. (2007).

[3] See http://galprop.stanford.edu.

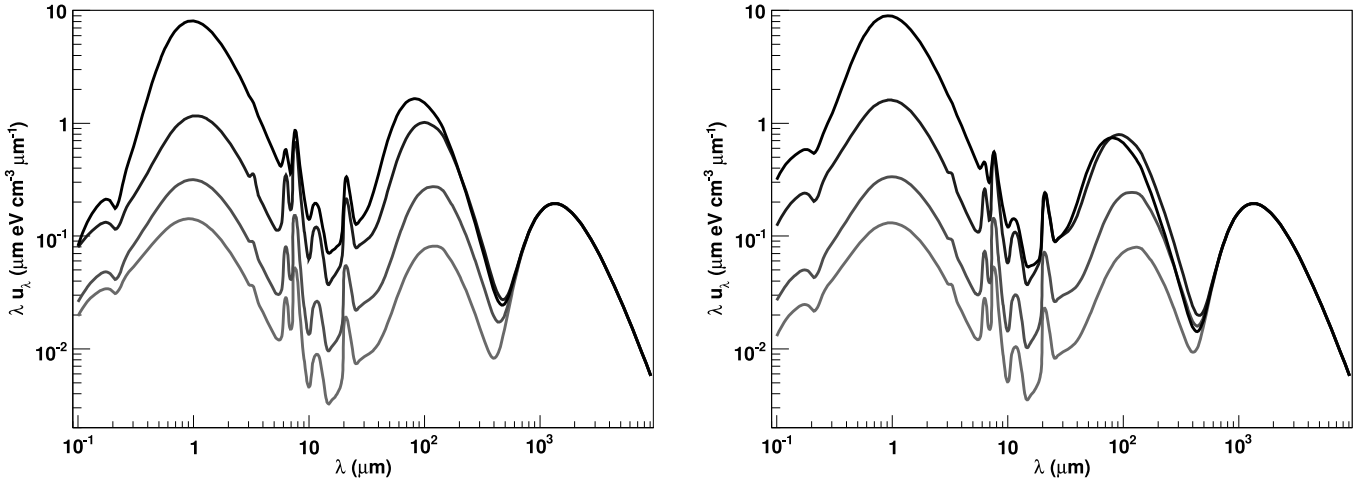

FIG. 1.— SED of the MW ISRF in the Galactic plane: $R = 0$ kpc, *black*; $R = 4$ kpc, *blue*; $R = 8$ kpc, *red*; and $R = 12$ kpc, *magenta*. *Left*: Maximum metallicity gradient, *Right*: Minimum metallicity gradient. The CMB is included in both figures and dominates the SED for wavelengths $\lambda \gtrsim 600$ μm. [*See the electronic edition of the Journal for a color version of this figure.*]

antiprotons). In this way secondaries, tertiaries, etc., are included. (Production of ^{10}B via the ^{10}Be-decay channel is important and requires a second iteration of this procedure.) GALPROP includes K-capture and electron stripping processes, where a nucleus with an electron (H-like) is considered a separate species because of the difference in lifetime, and knock-on electrons. Primary electrons are treated separately. Normalization of protons, alphas, and electrons to experimental data is provided (all other isotopes are determined by the source composition and propagation). Gamma rays are computed using interstellar gas data (for π^0-decay and bremsstrahlung) and the ISRF model (for IC). The synchrotron emission is computed using the Galactic magnetic field model. Spectra of all species on the chosen grid and the γ-ray and synchrotron sky maps are output in standard astronomical formats for comparison with data. Recent extensions to GALPROP include nonlinear wave damping (Ptuskin et al. 2006) and a dark matter package to allow for the propagation of WIMP annihilation products and calculation of the corresponding synchrotron and γ-ray sky maps; an interface between GALPROP and the DarkSUSY code (Gondolo et al. 2004) will be implemented in the near future to allow direct calls of GALPROP from within DarkSUSY.

The optimized model (Strong et al. 2004b) is used to calculate the diffuse emission in the range 10 keV–TeV energies. The CR source distribution is based on the Galactic pulsar distribution (Lorimer 2004), while the $X_{\rm CO}$-factors, $X_{\rm CO} = N({\rm H_2})/W_{\rm CO}$, are variable, increasing toward the outer Galaxy, and fully compatible with the expected variations based on the metallicity gradient and *COBE* data (Strong et al. 2004d). Such a model reproduces the diffuse Galactic γ-ray emission for the whole sky as well as the radial gradient of diffuse Galactic γ-ray emissivity.

3. INTERSTELLAR RADIATION FIELD

The Galactic ISRF is the result of emission by stars, and the scattering, absorption, and reemission of absorbed starlight by dust in the ISM. The most detailed calculation to date (Strong et al. 2000), which includes spatial and wavelength dependence over the whole Galaxy, has been widely used. The Strong et al. (2000) model uses emissivities based on stellar populations based on *COBE* DIRBE fits by Freudenreich (1998) and the SKY model of Wainscoat et al. (1992) together with *COBE* DIRBE derived infrared emissivities (Sodroski et al. 1997; Dwek et al. 1997). Subsequent to this work new relevant astronomical information on stellar populations, Galactic structure, and interstellar dust has become available, motivating a reevaluation of the ISRF. We briefly describe our calculation of the ISRF; further details can be found in Moskalenko et al. (2006) and Porter et al. (2006).

The fundamental factors influencing the ISRF are the luminosity distribution from the stellar populations of the Galaxy and the radiative transport of the star light through the ISM. The interstellar dust absorbs and scatters the star light in the ultraviolet (UV) and optical, and re-emits the absorbed radiation in the infrared.

In our model, we represent the stellar distribution by four spatial components: the thin and thick disk, the bulge, and the spheroidal halo. We follow Garwood & Jones (1987) and Wainscoat et al. (1992) and use a table of stellar spectral types comprising normal stars and exotics to represent the luminosity function (LF) for each of the spatial components. The spectral templates for each stellar type are taken from the semiempirical library of Pickles (1998). The normalizations per stellar type are obtained by adjusting the space densities to reproduce the observed LFs in the *V*- and *K*-band for the thin disk. The LFs for the other spatial components are obtained by adjusting weights per component for each of the stellar types relative to the normalizations obtained for the thin disk LF.

We assume a dust model including graphite, polycyclic aromatic hydrocarbons (PAHs), and silicate. Dust grains in the model are spherical and the absorption and scattering efficiencies for graphite, PAHs, and silicate grains are taken from Li & Draine (2001). The dust grain abundance and size distribution are taken from Weingartner & Draine (2001, their best-fit Galactic model). We assume a purely neutral ISM. We consider only coherent scattering, and a Henyey-Greenstein angular distribution function (Henyey & Greenstein 1941) is used in the scattering calculation. The stochastic heating of grains smaller than $\sim$0.1 μm is treated using the "thermal continuous" approach of Draine & Li (2001); we calculate the equilibrium heating of larger dust grains by balancing absorption with re-emission as described by Li & Draine (2001).

Dust follows the Galactic gas distribution, and we assume uniform mixing between the two in the ISM (Bohlin et al. 1978). The dust-to-gas ratio scales with the Galactic metallicity gradient. Estimates for the Galactic [O/H] gradient vary in the range 0.04–0.07 dex kpc^{-1} (Strong et al. 2004d and references therein). The variation of the metallicity gradient influences the redistribution of the mainly UV and blue component of the ISRF into

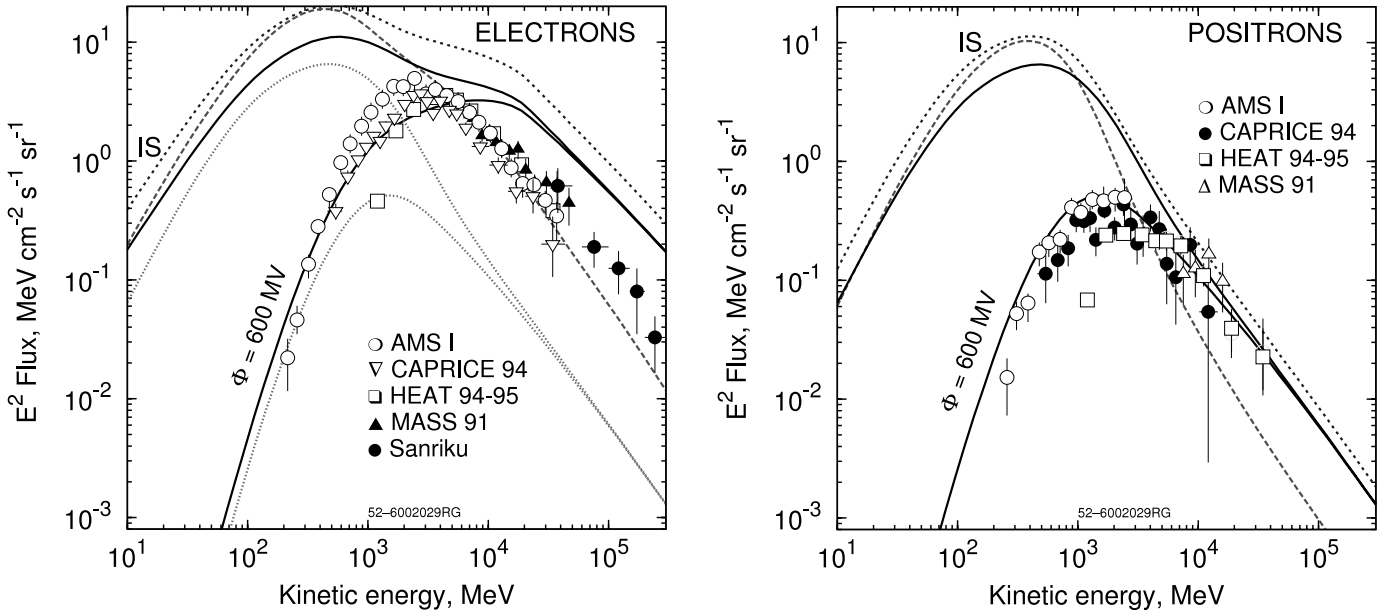

FIG. 2.—Spectra of CR electrons and positrons in the Galactic plane, as predicted by the adopted optimized GALPROP model. *Left*: Total (primary+secondary) and secondary electrons; *Right*: Secondary positrons. Interstellar spectra (IS): $R = 0$ kpc (*long-dashed line*), $R = 4$ kpc (*short-dashed line*), $R = 8.5$ kpc (*black solid line*), also shown modulated to 600 MV. Secondary electrons are shown separately as magenta lines (IS and modulated) on the left panel at $R = 8.5$ kpc. [*See the electronic edition of the Journal for a color version of this figure.*]

the infrared: increased metallicity implies more dust, which enhances the absorption of the star light. The variation in the infrared component affects the emission in the hard X-rays (see below). Therefore, we consider two ISRFs corresponding to a maximal case of 0.07 dex kpc^{-1} and a minimal case with no gradient.

The ISRF is calculated for a cylindrical geometry with azimuthal symmetry. The maximum radial extent is $R_{\rm max} = 20$ kpc with the maximum height above the galactic plane $z_{\rm max} = 5$ kpc. The radiative transport is performed using the so-called partial intensity method (Kylafis & Bahcall 1987; Baes & Dejonghe 2001).

Figure 1 shows the spectral energy distributions (SEDs) in the Galactic plane for selected galactocentric radii for the maximal metallicity gradient (*left*) and no metallicity gradient (*right*). An increased metallicity gradient reduces the UV in the inner Galaxy significantly—by up to a factor of 3 for $\lambda \lesssim 0.3$ μm—which is redistributed into the infrared. The infrared emission for the inner Galaxy for the maximum metallicity gradient is a factor of $\sim$2 higher than for the case of no metallicity gradient. For the outer Galaxy the ISRFs calculated for the two cases differ less dramatically. For the case of the maximal metallicity gradient the UV emission is higher than the no gradient case because there is less dust in the outer Galaxy. In turn, this results in less emission in the infrared than for the maximal gradient case.

4. RESULTS

We compare our results for the diffuse emission in the inner Galaxy with the new SPI data, and COMPTEL and EGRET data. The spectrum for each instrument is obtained by integrating over deconvolved sky maps. Since the deconvolution of the data is done based on the individual instrument response, cross-calibration of the data between the individual instruments is not an issue.

Our comparison with the SPI data is with the diffuse emission power-law component from Bouchet et al. (2008). We describe the procedure used to obtain the diffuse emission and how we estimate the uncertainty on this component. In the method of Bouchet et al. (2008) a source catalog is constructed using an iterative algorithm taking into account variable source flux contributions using templates for the spatial morphologies of the interstellar emission: 8° Gaussian for the positron annihilation emission, and DIRBE 4.9 μm and CO maps for the continuum below and above 120 keV, respectively. The normalization factor for each of these maps is adjusted during the fitting procedure. Following this initial step, the source fluxes and template information are discarded with only the source localizations retained. The source position information is used in the next step of the analysis where the region $|l| \leq 100^\circ$ and $|b| \leq 30^\circ$ is divided into cells with sizes that are chosen to optimize the signal-to-noise ratio per cell, while still being sufficiently small to follow the observed spatial variations. A likelihood fit is done using the a priori source position information to obtain the source fluxes and diffuse emission for each "pixel" cell over the energy ranges 25–50, 50–100, 100–200, 200–600, 600–1800, and 1800–7800 keV, respectively. This model independent "image-based" method establishes the extent of the diffuse emission. To extract the diffuse spectrum with a better signal-to-noise ratio, the background templates (DIRBE 4.9 μm, CO) are also fit for each energy range. The power-law continuum is based on this model-dependent method, but there is some error associated with the derived emission in this case which is not directly estimated in Bouchet et al. (2008). To estimate the effect on the diffuse emission, we compare the integrated latitude profiles obtained using the image-based method and the fit results for the background template maps given in Figure 5 of Bouchet et al. (2008). We conclude that the intensities could be up to 40% higher than the background template ones used by Bouchet et al. (2008) to construct their spectrum.

The primary electron and secondary positron and electron spectra from our propagation calculations are shown in Figure 2. For energies $\lesssim$1 GeV, the combined secondary positron and electron flux in the ISM actually exceeds the primary electron flux. This is due to the large ratio of CR nuclei to primary electrons. The addition of the secondary electrons and positrons increases by $\sim$2.5 the total number capable of producing γ-rays via IC scattering relative to the pure primary electrons.

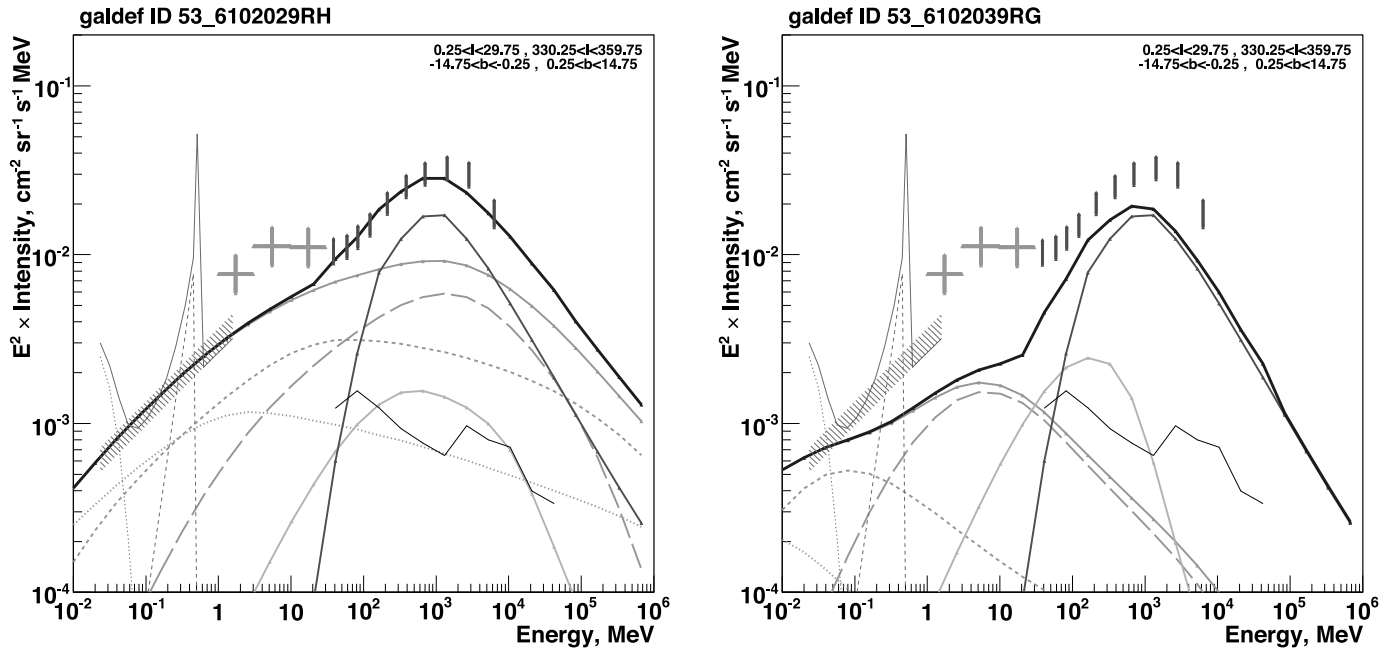

FIG. 3.—Spectrum of the diffuse emission for $330^\circ < l < 30^\circ, |b| < 15^\circ$ as calculated in the optimized GALPROP model for the ISRF with maximal metallicity gradient, with primary electrons only (*left*), and with secondary electrons and positrons only (*right*): π^0 decay, *red solid line*; IC (optical), *green long-dashed line*; IC (IR), *green short-dash line*; IC (CMB), *green dotted line*; total IC, *green solid line*; bremsstrahlung, *cyan solid line*; extragalactic γ-ray background (Strong et al. 2004a), *black solid line*; and total, *blue solid line*. Red data points are for EGRET, and green data points are for COMPTEL, as in Strong et al. (2005); magenta data points are for *INTEGRAL* SPI (*broken lines*: components in fit to positronium + positron annihilation line + unresolved point sources; *shaded region*: power-law continuum) Bouchet et al. (2008). For the SPI power-law continuum the uncertainty is estimated as described in the text. In this and subsequent figures, the identifier (e.g., 53_6102029RH) corresponds to the GALPROP version and run used; all parameters of the model are contained in the "GALDEF" parameter file for future reference and are available from the GALPROP World Wide Web site at http://galprop.stanford.edu. [*See the electronic edition of the Journal for a color version of this figure.*]

Figure 3 shows the individual contributions by primary electrons (*left*) and secondary electrons/positrons (*right*) to the diffuse Galactic emission. For primary electrons, the agreement with the SPI data is excellent while there is still some deficit when compared with COMPTEL. For secondary electrons and positrons, the spectrum of γ-rays is steeper below $\sim$10 MeV compared to the primary electrons, which is a reflection of the different source spectra: the primary electron source spectrum is found from adjusting to the γ-ray spectrum at higher energies, while the secondary electron/positron source spectrum follows from the CR nucleon spectrum in the ISM. The leptonic component at low energies (IC, bremsstrahlung) is thus intrinsically connected with the higher energy hadronic component (π^0-decay).

The components of the IC emission (Fig. 3) show the contributions by the ISRF components in different energy ranges. For primary electrons, the scattering of optical photons is the major contribution in the energy range $\sim$50 MeV–100 GeV, with the infrared the major component below $\sim$50 MeV and above 100 GeV, and the cosmic microwave background (CMB) comparable to the infrared below $\sim$500 keV. For the secondary electrons/positrons the scattering of the optical component dominates above $\sim$500 keV, while the infrared is the major component for energies below this. Thus, the primary and secondary populations IC scatter the components of the ISRF to different hard X-ray/γ-ray ranges. Interestingly, for secondary electrons/positrons the bremsstrahlung contribution is a factor $\sim$2 higher for 100 MeV to 1 GeV than the primary electron case. This reflects the enhancement of the electrons and positrons in the ISM below 1 GeV that was discussed in conjunction with Figure 2.

In Figure 4 we show the diffuse emission calculated using the optimized model with an ISRF calculated with a maximal metallicity gradient. Inverse Compton scattering is a major component at all energies, with π^0-decay more important between 100 MeV and 10 GeV, while the bremsstrahlung contribution is minor. The inclusion of secondary electrons and positrons increases the IC emission below $\sim$100 MeV by up to a factor $\sim$2, an effect that was pointed out by Strong et al. (2004b). Interestingly, the agreement with the COMPTEL data is improved by the inclusion of the secondary electrons/positrons, although the model still shows a deficit. Instead

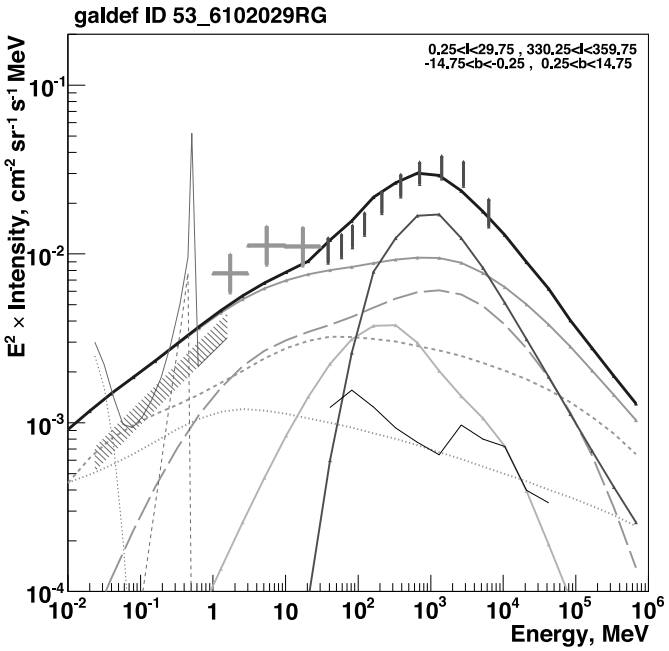

FIG. 4.—Total spectrum of the diffuse emission as calculated in the optimized model for $330^\circ < l < 30^\circ, |b| < 15^\circ$ with the maximum metallicity gradient. Line and data styles as for Fig. 3. [*See the electronic edition of the Journal for a color version of this figure.*]

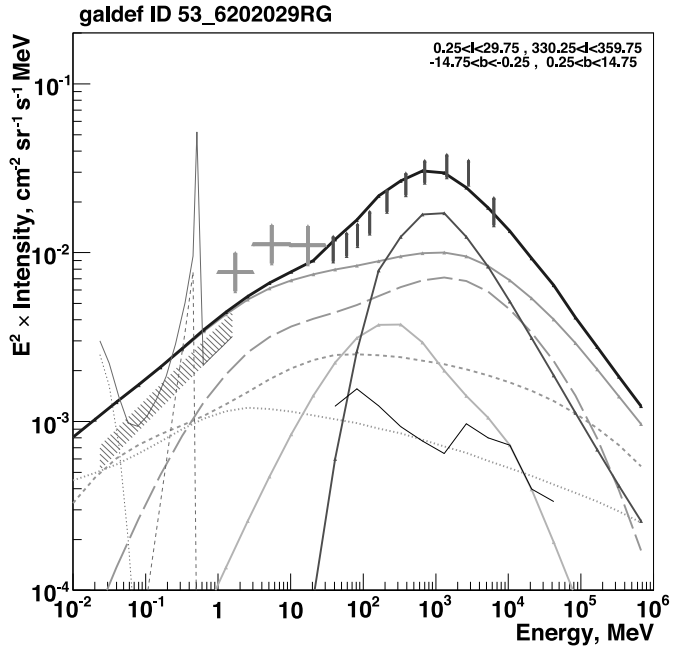

FIG. 5.—Spectrum of the diffuse emission as calculated in the optimized model with contribution of secondary electron and positrons and ISRF without the metallicity gradient. Region $330^\circ < l < 30^\circ, |b| < 15^\circ$. Line and data styles as in Fig. 4. [*See the electronic edition of the Journal for a color version of this figure*.]

the SPI data are overpredicted, but the spectral slope is still consistent with the data below 1 MeV given the estimated uncertainties. Since the secondary electrons/positrons are a by-product of the same processes that produce the π^0-decay γ-ray emission at higher energies, this may indicate that the ratio of CR nuclei to primary electrons we use in the ISM is too high. A possible remedy to recover the model fit if the CR nuclei to primary electron ratio is reduced could be that we have simply underestimated the optical component of the ISRF. If the CR nuclei flux is reduced to improve the agreement with SPI the model emission in the EGRET energy range would also be reduced. The emission in the MeV energy range comes from secondary electrons/positrons IC scattering the optical component of the ISRF, and primary electrons IC scatter the same component to GeV energies. Increasing the optical ISRF would simultaneously increase the emission in the MeV and GeV range, recovering the agreement of the model with EGRET data and possibly further improving the agreement with COMPTEL.

To test the dependence of the sub-MeV emission on the assumed ISRF model, we calculate the diffuse emission for the case of no metallicity gradient. Figure 5 shows the spectrum of the diffuse emission for this case. The major change in the ISRF is a ~30% reduction in the infrared emission which is due to the smaller amount of dust in the inner Galaxy when using this ISRF model. This results in a drop of ~10%–15% for the predicted intensity of the diffuse emission below ~1 MeV relative to the maximal gradient case. The optical emission increases only slightly, while the CMB emission stays the same. The total spectrum of the diffuse emission does not change significantly under this variation of the ISRF showing the robustness of the calculations.

We point out that the reduction in the infrared significantly reduces the contribution by secondary electrons and positrons to the total emission below a few hundred keV. In this energy range the emission by primary electrons is also reduced, but by a smaller amount because there is still a contribution by IC scattering of the CMB (see Fig. 3). Since the CMB is known, and if the infrared component of the ISRF is low, the emission below a hundred keV traces the primary electron spectrum in the ISM.

We have made our principal comparison with the spectrum for $|b| < 15^\circ$ since this is the nominal range for the spectrum presented in Bouchet et al. (2008). To illustrate the effect of different latitude ranges, we calculate the diffuse emission for $|b| < 10^\circ$ and $|b| < 5^\circ$ and compare with the data for these ranges. The results for these latitude ranges are shown in Figure 6. Since the extraction of the diffuse component from the SPI data relies on

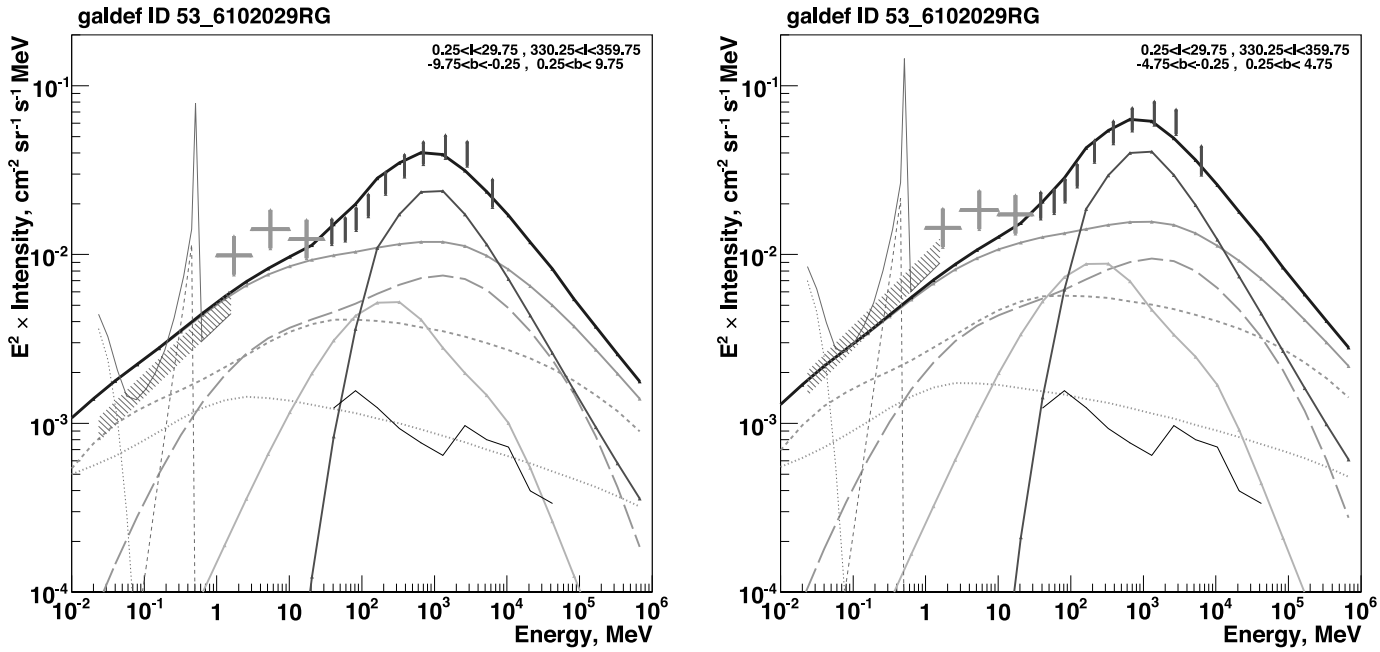

FIG. 6.—Spectrum of the diffuse emission as calculated in the optimized model with contribution of secondary electron and positrons for different latitude ranges. *Left*: Region $330^\circ < l < 30^\circ, |b| < 10^\circ$ *Right*: Region $330^\circ < l < 30^\circ, |b| < 5^\circ$. Line and data styles as in Fig 4 . [*See the electronic edition of the Journal for a color version of this figure*.]

templates whose latitude distribution may not exactly match the true distribution of the emission some of the signal may be absorbed into the baseline (see Fig. 5 of Bouchet et al. 2008). This introduces further uncertainty when comparing reduced latitude ranges which is difficult to quantify better than we have already done. The model emission is qualitatively similar to the data for the reduced latitude ranges, which points the way to using the IC emission as a template in future analyses of the SPI data.

5. DISCUSSION AND CONCLUSIONS

The agreement of the single model over the whole energy range from SPI data at low energies, to the EGRET data at high energies, is remarkable. Note that we are using the "optimized model" (Strong et al. 2004b), which has higher primary CR electron fluxes than observed locally, and also higher CR nuclei fluxes, as required to fit the γ-ray data above 30 MeV. With this model we predict too much emission below 1 MeV but seem to reproduce the spectral slope. Reducing the CR nuclei source spectrum to improve the sub-MeV agreement is a possibility. However it cannot be reduced too much since the local CR antiproton fluxes must still be reproduced by the model.[4] Increasing the optical component of the ISRF could improve the agreement at MeV and GeV energies. Variation of the primary electron injection index below a few GeV is another possible remedy to the overproduction of diffuse emission below 1 MeV. This requires a different source spectrum than is presently used in the optimized model to sufficiently reduce the sub-MeV diffuse emission in order to be consistent with the SPI spectrum. If instead we use the "conventional" model (Strong et al. 2004b) the situation will not be improved: the sub-MeV emission will be lower, but the agreement with the COMPTEL and EGRET data will be substantially worse.

There is still room for a contribution from populations of unresolved compact sources, particularly anomalous X-ray pulsars and radio pulsars, which may have very hard spectra extending to a few hundred keV (Kuiper et al. 2006). They may be responsible for the apparent peak near $b = 0^\circ$ in the Bouchet et al. (2008) latitude profiles.

The hard X-ray continuum is consistent with the predictions in both intensity and spectral index. However, the uncertainties in the model are still considerable: the distribution of CR sources and gas in the inner Galaxy which affect both the primary and secondary electrons/positrons, and the optical and infrared part of the ISRF (the CMB is of course known exactly). In fact, our optimized model overpredicts the SPI data, which could simply reflect these uncertainties, but the agreement in the spectral shape gives confidence that the mechanism is correctly identified.

There is still an excess in the COMPTEL energy range between 1 and 30 MeV which is to be explained. The contribution of the positron annihilation in flight may contribute in this energy range (Beacom & Yüksel 2006), but it has to be tested against the intensity of the 511 keV line and positronium continuum.

From our modeling, we find that the total rate of secondary positron production by CRs in the whole Galaxy is $\sim 2 \times 10^{42}$ s^{-1} in the optimized model. The conventional model gives a factor of $\sim$2 less positrons. These values are $\sim$10% of the positron annihilation rate $\sim 1.8 \times 10^{43}$ s^{-1} as derived from *INTEGRAL* observations of the 511 keV line emission (Knödlseder et al. 2005). The current CR flux of positrons is not sufficient to account for the observed annihilation rate. A CR origin for the 511 keV annihilation line could be reconciled with the production rate if CR intensities in the past were higher.

Our work illustrates the intrinsic connection between the diffuse Galactic γ-ray emission in different energy ranges. Inverse Compton emission by CR electrons and positrons on starlight and infrared radiation are the most important components of the hard X-ray and γ-ray emission in the 100 keV to few MeV range. A considerable proportion of this emission is produced by secondary electrons and positrons, the spectrum of which depends on the CR nuclei spectrum at energies $\sim$few GeV and higher. These CRs also produce π^0-decay γ-rays that dominate the emission in the *GLAST* range from 100 MeV to $\sim$10 GeV. Hence, *GLAST* observations of the π^0-decay diffuse emission will also constrain in the future the contribution by secondary electrons/positrons to the diffuse γ-ray emission in the SPI energy range. With the secondary electrons/positrons fixed, SPI observations probe the IC emission of primary CR electrons with energies $\lesssim$10 GeV scattering the infrared component of the ISRF and the CMB. This will provide information on the low-energy spectrum of primary CR electrons and the infrared component of the ISRF. In turn, since most of the diffuse γ-ray emission between $\sim$10 GeV–10 TeV is produced via IC scattering of primary electrons on the same starlight and infrared photons, this provides a connection to observations of diffuse emission at TeV energies by H.E.S.S. (Aharonian et al. 2006) and Milagro (Abdo et al. 2007).

[4] The BESS-Polar flight of 2004 (Abe et al. 2008) revealed that the CR antiproton flux is somewhat lower than previous measurements with lower statistics. If these data are confirmed, the CR proton spectrum will become better constrained. In turn, it will lead to a somewhat smaller flux of secondary leptons and improved agreement with the *INTEGRAL* data.

T. A. P. acknowledges partial support from the US Department of Energy. I. V. M. acknowledges partial support from NASA Astronomy and Physics Research and Analysis Program (APRA) grant.

REFERENCES

Abdo, A., et al. 2007, ApJ, 658, L33
Abe, K., et al. 2008, Phys. Lett. B, submitted (arXiv:0805.1754)
Aharonian, F., et al. 2006, Nature, 439, 695
Baes, M., & Dejonghe, H. 2001, MNRAS, 326, 722
Beacom, J. F., & Yüksel, H. 2006, Phys. Rev. Lett., 97, 071102
Berezinskii, V. S., et al. 1990, Astrophysics of Cosmic Rays, ed. V. L. Ginzburg (Amsterdam: North Holland)
Bleach, R. D., et al. 1972, ApJ, 174, L101
Bohlin, R. C., Savage, B. D., & Drake, J. F. 1978, ApJ, 224, 132
Bouchet, L., et al. 2005, ApJ, 635, 1103
———. 2008, ApJ, 679, 1315
Dermer, C. D. 1986a, ApJ, 307, 47
———. 1986b, A&A, 157, 223
Dogiel, V. A., et al. 2002, A&A, 382, 730
Draine, B. T., & Li, A. 2001, ApJ, 551, 807
Dwek, E., et al. 1997, ApJ, 475, 565
Ebisawa, K., et al. 2001, Science, 293, 1633
———. 2005, ApJ, 635, 214
Freudenreich, H. T. 1998, ApJ, 492, 495
Garwood, R., & Jones, T. J. 1987, PASP, 99, 453
Gondolo, P., et al., J. 2004, Cosmol. Astropart. Phys., 7, 8
Hands, A. D. P., et al. 2004, MNRAS, 351, 31
Henyey, L. G., & Greenstein, J. L. 1941, ApJ, 93, 70
Hunter, S. D., et al. 1997, ApJ, 481, 205
Kamae, T., et al. 2005, ApJ, 620, 244
Kaneda, H., et al. 1997, ApJ, 491, 638
Kelner, S. R., et al. 2006, Phys. Rev. D, 74, 034018
Kinzer, R. L., et al. 1999, ApJ, 515, 215
———. 2001, ApJ, 559, 282
Knödlseder, J., et al. 2005, A&A, 441, 513
Koch, H. W., & Motz, J. W. 1959, Rev. Mod. Phys., 31, 920
Koyama, K., et al. 1986, PASJ, 38, 503

Krivonos, R., et al. 2007, A&A, 463, 957
Kuiper, L., et al. 2006, ApJ, 645, 556
Kylafis, N. D., & Bahcall, J. N. 1987, ApJ, 317, 637
Lebrun, F. 2004, Nature, 428, 293
Li, A., & Draine, B. T. 2001, ApJ, 554, 778
Lorimer, D. R. 2004, Proc. COSPAR, 35, 1321
Mashnik, S. G., et al. 2004, Adv. Space Res., 34, 1288
Michelson, P. F. 2007, in AIP Conf. Proc., 921, First Int. *GLAST* Symp., ed. Ritz, S., et al. (Melville: AIP), 8
Moskalenko, I. V., Porter, T. A., & Strong, A. W. 2006, ApJ, 640, L155
Moskalenko, I. V., & Strong, A. W. 1998, ApJ, 493, 694
———. 2000, ApJ, 528, 357
Moskalenko, I. V., Strong, A. W., & Reimer, O. 2004, in Cosmic Gamma-Ray Sources, ed. K. S. Cheng & G. E. Romero, (Dordrecht: Kluwer), 279
Moskalenko, I. V., et al. 2002, ApJ, 565, 280
———. 2007, Nucl. Phys. B. Suppl., 173, 44
Pickles, A. J. 1998, PASP, 110, 863
Porter, T. A., Moskalenko, I. V., & Strong, A. W. 2006, ApJ, 648, L29
Press, W. H., et al. 1992, Numerical Recipes in FORTRAN: The Art of Scientific Computing (2nd ed.; Cambridge Cambridge Univ. Press)
Ptuskin, V. S., et al. 2006, ApJ, 642, 902
Purcell, W. R., et al. 1996, A&AS, 120, 389
Revnivtsev, M., & Sazonov, S. 2007, A&A, 471, 159
Revnivtsev, M., et al. 2006, A&A, 452, 169
Revnivtsev, M., et al. 2007, A&A, 473, 857
Ritz, S. 2007, in AIP Conf. Proc., 921, First Int. *GLAST* Symp., ed. S. Ritz, et al. (Melville: AIP), 3
Seo, E. S., & Ptuskin, V. S. 1994, ApJ, 431, 705
Sodroski, T. J., et al. 1997, ApJ, 480, 173
Strong, A. W. 2003, A&A, 411, L127
Strong, A. W., & Moskalenko, I. V. 1998, ApJ, 509, 212
Strong, A. W., Moskalenko, I. V., & Ptuskin, V. S. 2007, Annu. Rev. Nucl. Part. Sci., 57, 285
Strong, A. W., Moskalenko, I. V., & Reimer, O. 2000, ApJ, 537, 763
———. 2004a, ApJ, 613, 956
———. 2004b, ApJ, 613, 962
Strong, A. W., et al. 2003, A&A, 411, L447
———. 2004c, in Proc. 5th *INTEGRAL* Workshop, ed. V. Schönfelder, G. Lichti & C. Winkler (ESA SP-552; Noordwijk: ESA), 507
———. 2004d, A&A, 422, L47
———. 2005, A&A, 444, 495
Terrier, R., et al. 2004, in Proc. 5th *INTEGRAL* Workshop, ed. V. Schönfelder, G. Lichti & C. Winkler (ESA SP-552; Noordwijk: ESA), 513
Valinia, A., et al. 2000, ApJ, 543, 733
Wainscoat, R. J., et al. 1992, ApJS, 83, 111
Weingartner, J. C., & Draine, B. T. 2001, ApJ, 548, 296
Worrall, D. M., et al. 1982, ApJ, 255, 111
Yamasaki, N. Y., et al. 1997, ApJ, 481, 821